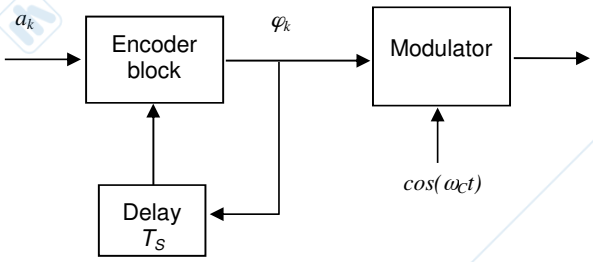

Figure 4.3: Scheme of a DPSK modulator.

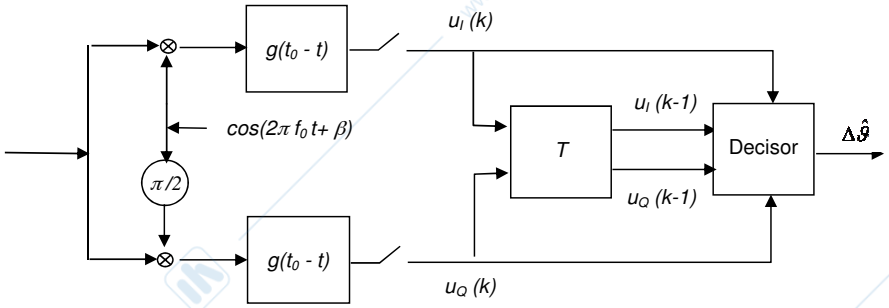

Figure 4.4: Scheme of a DPSK demodulator.

4.3 Single carrier modulations

In this Section, we will consider the most diffused families of modulation schemes for wireless communications. We assume that the standard modulations schemes as BPSK, PSK and QAM are known (for a review of these schemes, please refer to a book on digital communications).

4.3.1 Differential PSK

Differential PSK responds to the possibility of eliminating the phase recovery block at the receiver (Fig. 4.2), simplifying its architecture. The functioning principle is simple: instead of modulating the absolute phase of a carrier with the information symbols, here we associate each symbol to the difference of phase between a symbol and the successive one. At the receiver it is not necessary to recover the absolute carrier phase any more but it is enough to subtract the phase of the previous symbol from the current one. Therefore the receiver will be denoted as non-coherent. The drawback of this simple technique is the performance loss since the final decision will be taken on a sample derived by two noisy sources (the current symbol phase and the previous one)

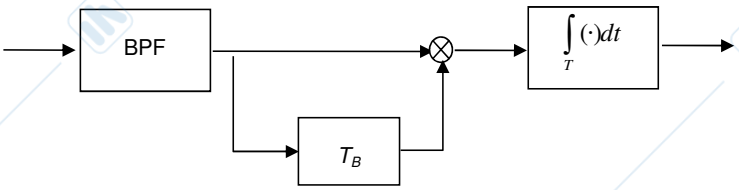

Figure 4.5: Simplified scheme of a binary DPSK demodulator.

instead of a single one (only the current symbol phase in the PSK case).

The general modulator is depicted in Fig. 4.3: the encoder block returns the current carrier phase according to the last two symbols; the phase $\phi_k = \phi_{k-1} + \Delta\phi_k$ modulates a carrier $Acos(2\pi f_C t + \phi_k)$ exactly as in the PSK case. The current symbol determines the phase increment $\Delta\phi_k$ (for example, in the binary case, 0 can be associated to $\Delta\phi_k = 0$ and 1 to $\Delta\phi_k = \pi$). The constellation and the bandwidth are exactly the same as PSK. The demodulator reported in Fig. 4.3 is characterized by the final decision block, which operates on two successive samples since it must recover the phase difference and associate it to the trasmitted symbol.

In the binary case the demodulator can be implemented also by a structure with a single branch, as reported in Fig. 4.5. It can be proved that performance in the binary case is only slightly worse than the coherent case BPSK and it is given by

$$P(E) = \frac{1}{2} e^{-E_B/N_0}, \tag{4.3.1}$$

where E_B and N_0 are the usual energy per bit and AWGN one-sided power spectral density respectively. In the non binary case ($M > 2$), the performance loss increases till to 3 dB w.r.t. the corresponding coherent M-PSK.

4.3.2 Offset QPSK and $\pi/4$-QPSK

In phase modulations (PSK, DPSK), when a symbol changes the signal is interested by a discontinuous phase transition, whose maximum absolute value $|\Delta\phi_k|$ is given by π. This maximum phase change corresponds to a sign inversion and, as can be seen easily in a signal constellation, to a so-called zero-crossing. This π transition is particularly damaging when the signal passes through a non-linear amplifier since, during the phase change (which cannot be instantaneous), the signal envelope cannot be considered constant anymore. Therefore the output signal turns out to be affected by distortion and spurious components in the spectrum. In order to limit

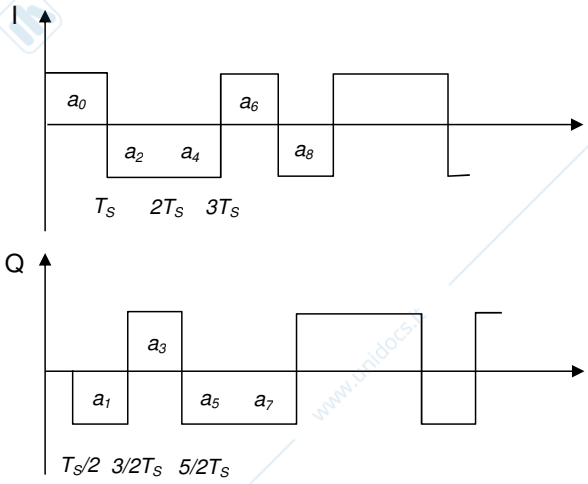

(a)

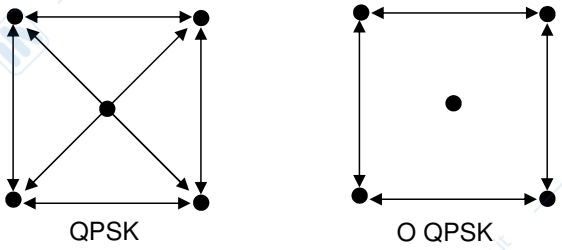

(b)

Figure 4.6: Offest QPSK: functioning principle (a) and phase transitions (b).

this effect in quaternary constellations, as QPSK and 4-DPSK, two modified schemes have been proposed: O-QPSK or offset QPSK and $\pi/4$-QPSK.

In O-QPSK, the two bit streams, associated to the direct and quadrature channels I and Q, are delayed each other of a time offset equal to $T_S/2 = T_B$ (Fig. 4.6(a)). By means of this expedient, it is easy to realize that now the transitions occur at multiple of $T_S/2$ (instead of T_S) but each transition is limited to a maximum phase discontinuity equal to $\pi/2$ (Fig. 4.6(b)). Performance and bandwidth are equal to the QPSK case.

In $\pi/4$-QPSK, the modulation is performed typically in a differential fashion, like in Table 4.1. The effect on the constellation is depicted in Fig. 4.7: at even multiples of T_S, the constellation is composed by the angles $\phi_k = n\pi/2$ (case (a)) while, at odd multiples of T_S, the constellation

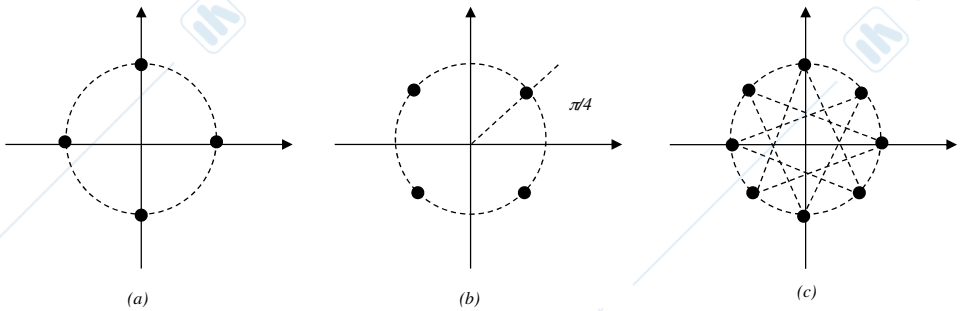

Figure 4.7: Constellations switch in $\pi/4$-QPSK (a) and (b). Overall phase transitions diagram in (c).

Bits	$\Delta\phi$
00	$\pi/4$
01	$3\pi/4$
11	$-3\pi/4$
10	$-\pi/4$

Table 4.1: Differential values of phases in $\pi/4$-QPSK.

is composed by the angles $\phi_k = n\pi/2 + \pi/4$ (case (b)). So the constellation switches between configurations (a) and (b), and the maximum phase transition $|\Delta\phi_k| = 3\pi/4$, which poses $\pi/4$-QPSK between OQPSK ($\pi/2$) and standard QPSK (π). However the main advantage of $\pi/4$-QPSK is its inherent differential nature, which makes possible the use of a non-coherent receiver.

4.3.3 FSK

In binary FSK, the current bit is associated to the two waveforms

$$s_0(t) = Ag(t)cos(2\pi f_0 t + \Phi_0) \tag{4.3.2}$$

and

$$s_1(t) = Ag(t)cos(2\pi f_1 t + \Phi_1) \tag{4.3.3}$$

with $g(t)$ typically assumed rectangular (of duration T equal to the symbol or bit time), for its constant envelope characteristics. In order to guarantee the orthogonality between the two pulses $s_0(t)$ and $s_1(t)$ (condition for obtaining the best performance and the simplest receiver) for each

phase (Φ_0 and Φ_1), the two frequencies f_0 and f_1 must respect the following condition

$$\Delta f = f_1 - f_0 = \frac{n}{T}, \tag{4.3.4}$$

that reduces to $\Delta f = 1/T$ for restricting the occupied bandwidth to the minimum. The interesting point of this modulation is the extreme simplicity of the modulator and of the demodulator, that can be composed by a couple of filters and envelope detectors in its non-coherent implementation (Fig. 4.8). In this case, the receiver filters the signal around the two frequencies and estimates the output energy content; the received bit is decided according to the signal with the maximum amount of energy. We observe that each branch of the receiver in Fig. 4.8 is equivalent to the scheme in Fig. 4.9, where it is evident the physical meaning of the output sample, equal to the square value of the energy received around f_0 (or f_1). Performance of non-coherent FSK binary demodulation has a formula similar to DPSK, with 3 dB performance loss,

$$P(E) = \frac{1}{2} e^{-E_B/(2N_0)}. \tag{4.3.5}$$

The 3 dB loss is maintained in the coherent demodulation (Fig. 4.10) w.r.t. BPSK. We have indeed

$$P(E) = Q\left(\sqrt{\frac{E_B}{N_0}}\right), \tag{4.3.6}$$

which has the same asymptotic behavior of (4.3.5), as in the DPSK case. The spectrum is not good especially when the pulse is rectangular and the two phases Φ_0 and Φ_1 are independent and not continuous.

Performance of FSK with M levels can be evaluated by means of the symbol error upper bound

$$P_S(E) \leq (M-1)P_2(E), \tag{4.3.7}$$

where $P_2(E) = Q\left(\sqrt{\frac{E_S}{N_0}}\right)$ or $\frac{1}{2}e^{-E_S/(2N_0)}$ is the error probability computed between each couple of symbols in the constellation in the coherent or non-coherent case.

4.3.4 Continuous phase FSK

The modulation schemes in Sect. 4.3.1, 4.3.2 and 4.3.3 are characterized, at least in principle, by constant envelope. However in these schemes the phase evolution is characterized by discontinuities (step transitions) at each symbol change and this affects heavily the resulting spectrum, which turns out to be typically interested by not negligible sidelobes and which is often not

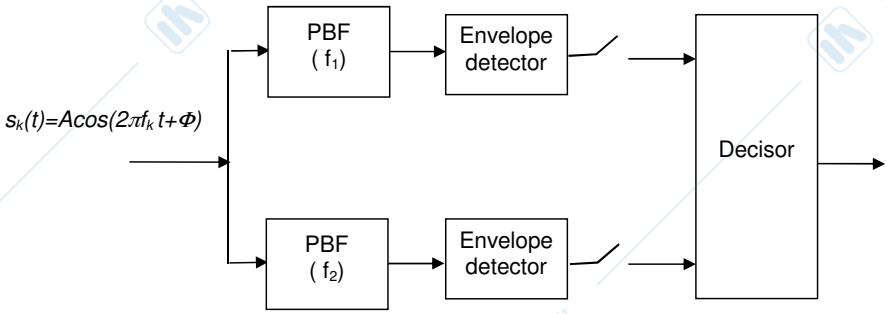

Figure 4.8: Non coherent demodulator for FSK.

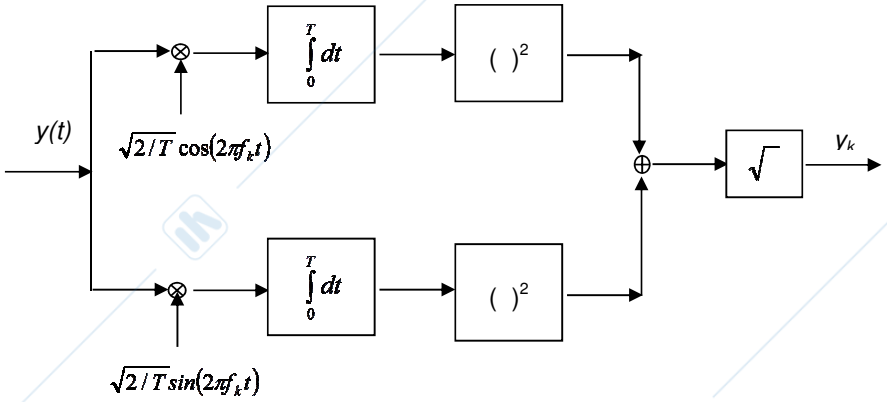

Figure 4.9: Equivalent structure for each branch of the non-coherent demodulator in Fig. 4.8.

enough compact for the most stringent channel bands requirements. In order to overcome the phase discontinuous transitions between successive symbols, it is possible to modulate the transmitted signal ensuring the phase continuity. This is obtained by means of a frequency modulator that operates on a pulses sequence linearly modulated by the information levels; in other words, if we modulate a single carrier frequency with a pulse train, the instantaneous carrier phase, being proportional to the integral of the instantaneous frequency, will turn out to be continuous. So, if the modulating pulse train is

$$d(t) = \sum_k I_k g(t - kT), \tag{4.3.8}$$

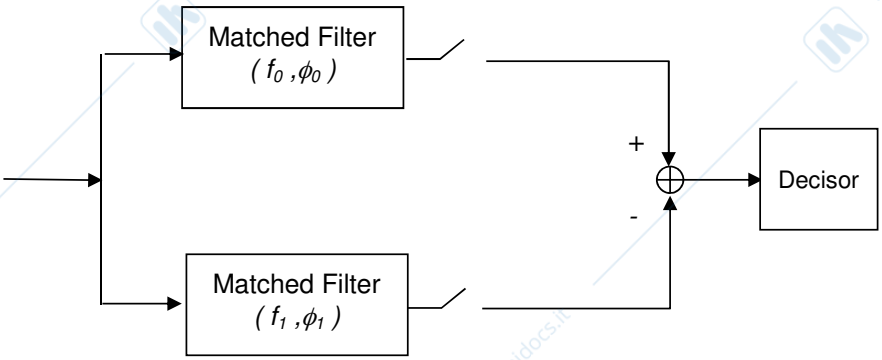

Figure 4.10: Coherent demodulator for FSK.

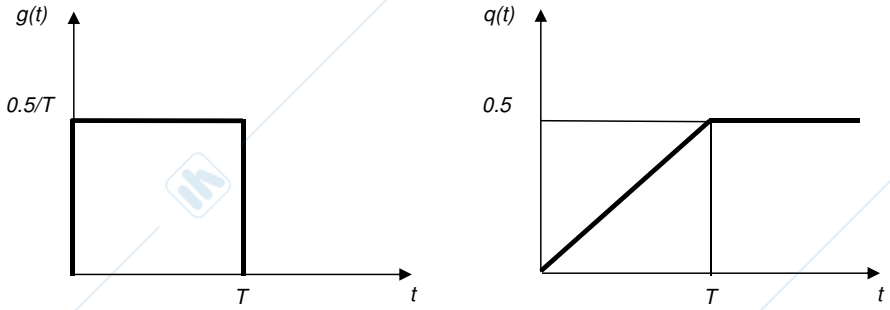

Figure 4.11: MSK modulating pulses $g(t)$ and $q(t)$.

where I_k are the modulation levels ($M = 2, 4, \cdots$), T is the symbol time and $g(t)$ the pulse used for modulating frequency, the modulated frequency will be proportional to $d(t)$, i.e.

$$f(t) = f_C + hd(t), \tag{4.3.9}$$

with the parameter h acting as the modulation index. The modulating pulse $g(t)$ can be limited between 0 and T (in this case the modulation is referred as 'full response' and $d(t)$ has no intersymbol interference) or not ('partial response'). In addition the pulse $g(t)$ is conventionally assumed to have area equal to 1/2. The resulting carrier $s(t)$ will be characterized by an instantaneous phase that is the integral of (4.3.9), namely

$$s(t) = Acos(\Phi(t)), \tag{4.3.10}$$

with

$$\Phi(t) = 2\pi \int_{-\infty}^{t} f(\tau)d\tau + \Phi_0 = 2\pi f_C t + 2\pi h \int_{-\infty}^{t} d(\tau)d\tau + \Phi_0. \tag{4.3.11}$$

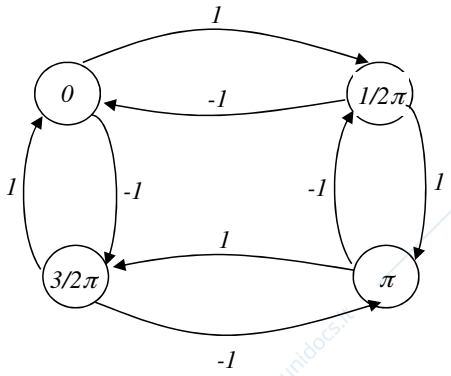

Figure 4.12: MSK state diagram.

If we restrict our attention on the component in (4.3.11) containing the information stream, we can easily write that

$$\Phi_I(t) = 2\pi h \sum_k I_k q(t - kT), \tag{4.3.12}$$

where $q(t) = \int_{-\infty}^{t} g(\tau)d\tau$ and it is now continuous. At the same time, (4.3.12) reveals that the phase continuity has increased the system complexity: now the current phase is a function not only of the current symbol but also of the past history, namely of the phase cumulated by the past symbols. If we consider a full response modulation we can express the phase in a generic time interval $kT \leq t \leq (k+1)T$ as

$$\Phi_I(t) = 2\pi h I_k q(t - kT) + \pi h \sum_{j=-\infty}^{k-1} I_j = 2\pi h I_k q(t - kT) + S_{k-1}, \tag{4.3.13}$$

where the term S_{k-1} represents the phase value achieved at the end of the $k-1$-th symbol. It is possible to see that, if h is rational ($h = m/n$), only a finite number of values in S_{k-1} are possible (n when m is even and $2n$ when m is odd): this set of values constitutes the set of possible states in which the system can be at the end of each symbol. Therefore the system is described by a state diagram in which each state represents its past history or memory (S_{k-1}) and the current transition is determined by the current symbol I_k.

For understanding better these concepts, let us consider the most important and known example of CPFSK modulation, i.e. the MSK (Minimum Shift Keying). Each CPFSK modulation is defined by the number of levels, the modulation index h and the pulse $g(t)$; for MSK we have:

- binary modulation, i.e. $I_k = \pm 1$;

- $h = 1/2$;
- rectangular pulse $g(t) = 1/(2T)$ between 0 and T and therefore $q(t)$ is a linear ramp $t/(2T)$ for $0 \leq t \leq T$, 0 for $t \leq 0$ and $1/2$ for $t \geq 0$ (Fig. 4.11).

These parameters produce the following phase trajectory

$$\Phi_I(t) = I_k \frac{\pi}{2} \frac{t - kT}{T} + \frac{\pi}{2} \sum_{j=-\infty}^{k-1} I_j \tag{4.3.14}$$

and it is easy to realize that the possible values of $S_{k-1} = \pi/2 \sum_{j=-\infty}^{k-1} I_j$ and hence the possible states of the modulation are 4, or $\{0, \pi/2, \pi, -\pi/2\}$. The resulting state diagram is reported in Fig. 4.12 and the phase evolution can be tracked in a trellis phase diagram which describes the possible phase trajectories as a function of time, as in Fig. 4.13(a). It is also possible to see that MSK is characterized by the minimum frequency difference compatible with the pulses orthogonality; deriving 4.3.11 and using (4.3.14), we obtain $f(t) = f_c \pm 1/(4T)$ and consequently $\Delta f = 1/(2T)$.

The MSK receiver has some interesting properties that make it a valid candidate for wireless transmission: as in the more general CPFSK schemes, the demodulator can be implemented in a non-coherent way (exploiting the FSK modulated data) achieving a similar performance in terms of bit error rate and in a coherent way, tracking the phase trajectories between the system states. Therefore, in general, a CPFSK demodulator will be characterized by a state machine that selects the most likely phase sequences (and the associated transmitted levels).

One of the most relevant peculiarities of MSK is the possibility of implementing a coherent receiver that has the same architecture of a QPSK demodulator, namely characterized by two branches and two independent decisors (Fig. 4.14). In order to understand how this architecture is designed, let us start from

$$s(t) = Acos(2\pi f_C t + \Phi_I(t)) = Acos(2\pi f_C t + 2\pi h I_k q(t - kT) + S_{k-1}) \tag{4.3.15}$$

and observe the following property of MSK phase evolution (Fig. 4.13): at even multiples of T $(0, 2T, 4T, \cdots)$ the phase (and the corresponding state) can assume only the values 0 and π while at odd multiples of T $(T, 3T, 5T, \cdots)$ the possible state values are $\pi/2$ and $-\pi/2$. Now let us restrict our attention, for the sake of simplicity, on the symbol period corresponding to $k = 0$, from $t = 0$ to T. In this time interval, $\Phi_I(t)$ can be written in two alternative forms:

- $\Phi_I(t) = \pm 2\pi hq(t-kT) + S_{k-1} = \pm\frac{\pi t}{2T} + \Phi_I(0)$, with $\Phi_I(0) = \{0, \pi\}$;
- $\Phi_I(t) = S_k - (\pm 2\pi hq(t-(k+1)T)) = \pm\frac{\pi(t-T)}{2T} + \Phi_I(T) = \pm\frac{\pi(t-T)}{2T} + \Phi_I(T)$, with $\Phi_I(T) = \{-\pi/2, \pi/2\}$.

We also observe that the validity of the former formulation can be extended from $-T \leq t \leq T$, centered on $\Phi_I(0)$, while the latter from $0 \leq t \leq 2T$, centered on $\Phi_I(T)$. Now we use the former formulation in writing the direct signal and the latter in the quadrature one, obtaining

$$\begin{aligned} s(t) &= A cos(2\pi f_C t) \cdot cos\left(\pm\frac{\pi t}{2T} + \Phi_I(0)\right) - A sin(2\pi f_C t) \cdot sin\left(\pm\frac{\pi(t-T)}{2T} + \Phi_I(T)\right) \\ &= A cos(2\pi f_C t)\left[cos\left(\pm\frac{\pi t}{2T}\right) cos\left(\Phi_I(0)\right) - sin\left(\pm\frac{\pi t}{2T}\right) sin\left(\Phi_I(0)\right)\right] + \\ &\quad - A sin(2\pi f_C t)\left[sin\left(\pm\frac{\pi(t-T)}{2T}\right) cos\left(\Phi_I(T)\right) + cos\left(\pm\frac{\pi(t-T)}{2T}\right) sin\left(\Phi_I(T)\right)\right] \\ &= A cos(2\pi f_C t) \cdot cos\left(\frac{\pi t}{2T}\right) cos\left(\Phi_I(0)\right) - A sin(2\pi f_C t) \cdot sin\left(\frac{\pi t}{2T}\right) sin\left(\Phi_I(T)\right) \end{aligned} \quad (4.3.16)$$

where, in the last step, we have exploited the following properties:

- $sin\left(\Phi_I(0)\right) = 0$ since $\Phi_I(0) = \{0, \pi\}$ and $cos\left(\Phi_I(T)\right) = 0$ since $\Phi_I(T) = \{-\pi/2, \pi/2\}$,
- $cos\left(\pm\frac{\pi t}{2T}\right) = cos\left(\frac{\pi t}{2T}\right)$,
- $cos\left(\pm\frac{\pi(t-T)}{2T}\right) = cos\left(\frac{\pi(t-T)}{2T}\right) = cos\left(\frac{\pi t}{2T} - \frac{\pi}{2}\right) = sin\left(\frac{\pi t}{2T}\right)$.

Similarly, if we move in the odd time intervals, i.e. from $t = T$ to $2T$, we obtain

$$s(t) = A cos(2\pi f_C t) \cdot cos\left(\frac{\pi(t-2T)}{2T}\right) cos\left(\Phi_I(2T)\right) - A sin(2\pi f_C t) \cdot sin\left(\frac{\pi t}{2T}\right) sin\left(\Phi_I(T)\right). \quad (4.3.17)$$

It is important to highlight that the information content in Equ. (4.3.16) and (4.3.17) is now in the amplitude levels of the direct and quadrature signals ($cos(\Phi_I(0)) = \pm 1$ and $-sin(\Phi_I(T)) = \pm 1$) and not in the signal phase anymore. Therefore the signal is represented by a direct and quadrature level modulation and it can be written as

$$s(t) = \sum_k c_k p(t-2kT) \cdot cos(2\pi f_C t) + \sum_k d_k p(t-(2k+1)T) \cdot sin(2\pi f_C t) \quad (4.3.18)$$

where $p(t) = cos\left(\frac{\pi t}{2T}\right)$, $c_k = cos(\Phi_I(2kT))$ and $d_k = -sin(\Phi_I((2k+1)T))$. So, using (4.3.16) and (4.3.17), the demodulator can obtain the estimates of the levels c_k and d_k, related to the trellis phases and hence to the information levels I_k, by means of a two-branches structure exactly

I_k	c_k, d_k	$\Phi_I(0)$, $\Phi_I(T)$
$+1$	$+1$, -1	0, $\pi/2$
-1	-1, -1	π, $\pi/2$
$+1$	-1, $+1$	π, $-\pi/2$
-1	$+1$, $+1$	0, $-\pi/2$

Table 4.2: Decoding table for MSK at even k ($2nT \leq t \leq (2n+1)T$). A similar table is used at odd k.

equivalent to a QPSK demodulator with shaping pulse $p(t)$. The only difference is the timing offset in the two branches. It is easy to realize that also performance is equivalent, i.e.

$$P(E) = Q\left(\sqrt{\frac{2E_B}{N_0}}\right), \tag{4.3.19}$$

since, on each branch, the probability of error is determined by the distance between the two levels $-\sqrt{E_B}$ and $\sqrt{E_B}$ (the energy of each pulse $p(t)$ corresponds to the energy per bit E_B). We can observe that, w.r.t. the non coherent implementation, we have here a performance advantage around 3 dB; this gap and the complexity comparable to the QPSK demodulator make this coherent implementation of MSK demodulator particularly appealing. The final decoding step of the demodulator in Fig. 4.14 is easy, as it consists of translating the streams c_k, d_k into the corresponding transmitted bits; this can be done by means of decoding tables, like that shown in Table 4.2. It is important to observe that the signal two-branch representation in (4.3.16) is exploited also for implementing the modulator: the bits are translated into the levels c_k, d_k, which modulate the pulse $p(t)$ with rate $1/(2T)$ and time offset T on the direct and quadrature channels.

A modified version of MSK has been investigated (and adopted, for example, in GSM), with the aim of improving further the spectral properties of the modulation. As we have already observed, the smoother the phase transition, the sharper the spectrum edges and hence the more compact the spectrum. This CPFSK modulation uses the same modulation index and levels of MSK but a different pulse $g(t)$, obtained by filtering the rectangular pulse $g_R(t)$ of duration T through a Gaussian filter with a specific -3 dB bandwidth B_G (Fig. 4.15). The impulse response of the Gaussian filter is

$$h(t) = \sqrt{\frac{2\pi}{ln2}} \cdot B_G \cdot e^{-\frac{2\pi^2 B_G^2 t^2}{ln2}} \tag{4.3.20}$$

and the corresponding transfer function is still Gaussian and equal to

$$H(f) = e^{-\frac{ln2}{2}\left(\frac{f}{B_G}\right)^2}. \tag{4.3.21}$$

The resulting modulation is called Gaussian MSK (GMSK) and it is characterized by the ratio between B_G and the 1^{st} zero bandwidth of the input rectangular pulse, i.e. $1/T$. It is clear that the larger is $B_G T$, the more $g(t)$ will be similar to $g_R(t)$ (for $B_G T \to +\infty$ GMSK reduces to MSK). However values of $B_G T$ smaller than one makes $g(t)$ smoother, with a positive impact on the spectrum compactness; the major drawback of this operation is that $g(t)$ tends to enlarge in the time domain, causing inter-symbol interference (ISI) among the phase contributions of the symbols sequence. The exact pulse waveform is given by

$$g(t) = rect\left(\frac{t}{T}\right) * h(t) = \frac{1}{2T}\left[Q\left(\frac{2\pi B_G}{\sqrt{ln2}}\left(t - \frac{T}{2}\right)\right) - Q\left(\frac{2\pi B_G}{\sqrt{ln2}}\left(t + \frac{T}{2}\right)\right)\right]. \tag{4.3.22}$$

The GMSK modulation adopted in GSM uses the factor $B_G T = 0.3$, which corresponds to a pulse $g(t)$ spread across 3 symbols instead of 1 (Fig. 4.16). The use of a pulse whose duration exceeds the symbol time (partial response CPFSK) has two practical consequences:

1. coherent and non-coherent performance decreases since ISI reduces the minimum Euclidean distance between the signals corresponding to competing phase trajectories.

2. The optimal detector (in particular the coherent one) is supposed to operate decisions not on single symbols (as in MSK) but on the entire sequence in order to solve the ISI components, which distribute their impact on more symbols.

In the GMSK case with $B_G T = 0.3$, the performance loss w.r.t. MSK is about 0.5 dB, which is an acceptable loss if we consider the advantageous resulting spectrum shape. It is also important to observe that GMSK modulation allows a sub-optimal receiver, whose architecture is similar to the MSK one (Fig. 4.17). The use of this sub-optimal demodulator, which takes advantage by the design of an additional input Gaussian filter, is made at the expense of an additional loss around 1 dB but it avoids the implementation of a more complicated sequence detector.

4.3.5 Power spectra of modulated signals

In this Sect. we report some numerical examples of the power spectra of digital modulations discussed in the past sections.

In linearly modulated signals, responding to an expression $s_L(t) = \sum_k a_k g(t - KT)$, as BPSK, M-PSK, QAM, the power spectral density, when $E[a_k] = 0$, is determined by the Fourier transform of the pulse. Therefore,

$$S_{PSD}(f) = \frac{\sigma_a^2}{T} \cdot |G(f)|^2, \tag{4.3.23}$$

where σ_a^2 is the power of the levels a_k. On th other hand, FSK with non coherent phases and orthogonal pulses ($\Delta f = 1/T$) can be seen as the superposition of two streams of levels $\{0, 1\}$ where $E[a_k] = 0.5$, so producing, in addition to the 2 sinc shaped pulses around $f = \pm 1/T$ (whose power spectral density decays as f^{-2}), also a train of train of spectral lines spaced of multiples of $1/T$:

$$S_{PSD}(f) = C[|sinc(fT - 0.5)|^2 + |sinc(fT + 0.5)|^2] + \sum_k D_k \delta\left(t - k/T\right). \tag{4.3.24}$$

For CPFSK modulations, the derivation of the spectral power density is generally more difficult; we report the formula for MSK, which is characterized by a first zero at $fT = 3/4$:

$$S_{PSD}(f) = C\left[\frac{cos(2\pi fT)^2}{16 \cdot f^2T^2 - 1}\right]^2. \tag{4.3.25}$$

Figs. 4.18, 4.19 report some examples of spectra for modulation with discontinuous phase and different pulses (the root raised cosine is an efficient choice but it has not constant envelope). Figs. 4.20 and 4.21 show the remarkable improvement provided by CPFSK modulation and, in particular, by the introduction of the Gaussian filter with different values of the parameter B_GT.

Finally, in Fig. 4.22, we report a comparison among the spectral efficiencies achieved by different modulations in order to appreciate the impact of a more compact spectrum.

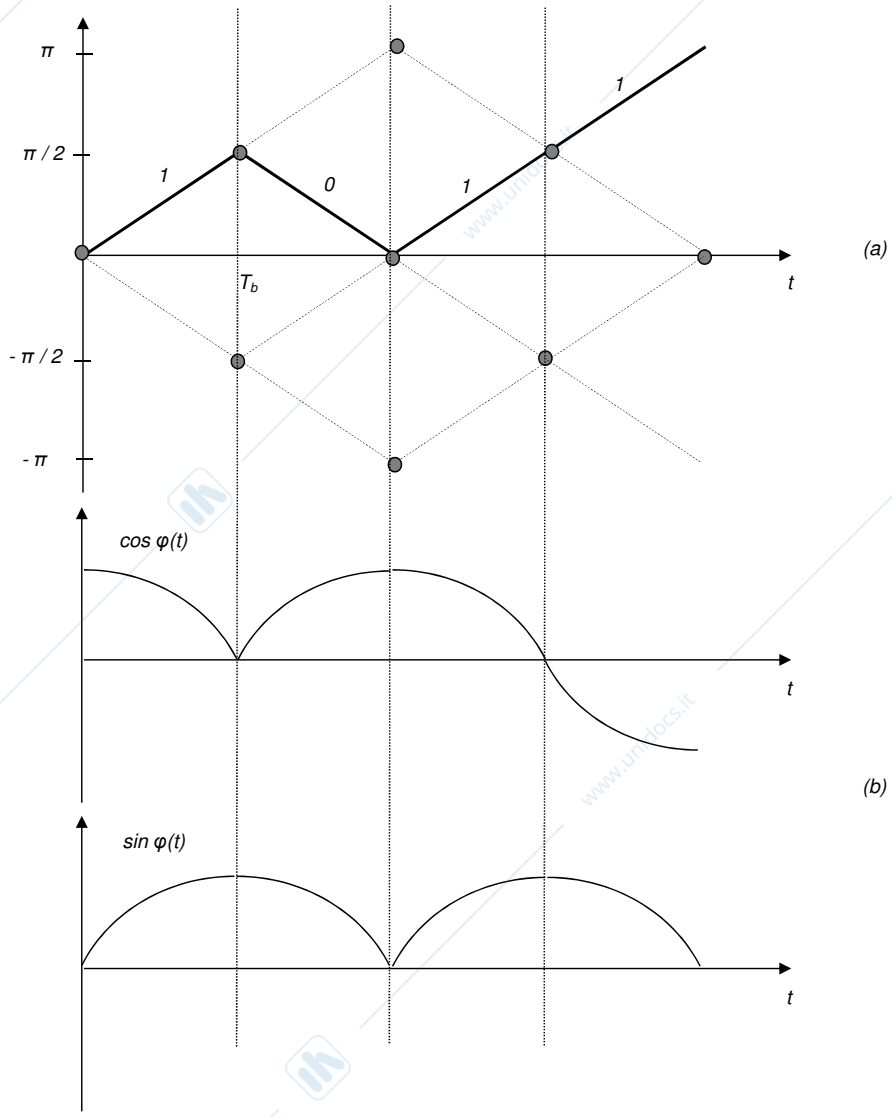

Figure 4.13: MSK phase trellis (a) and direct and quadrature pulses sequences (b).

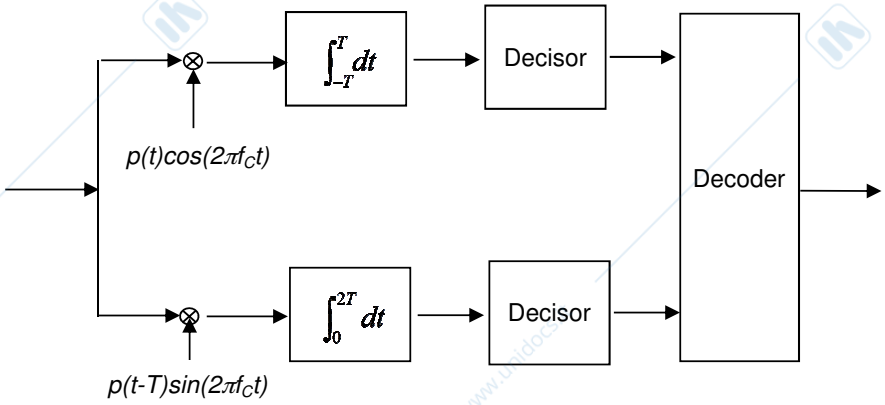

Figure 4.14: MSK coherent demodulator.

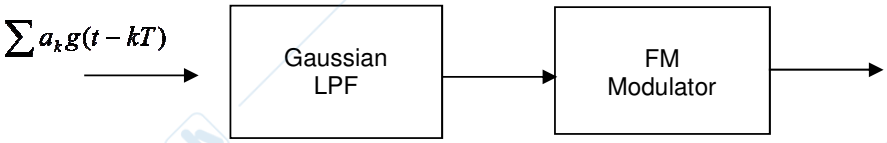

Figure 4.15: GMSK modulator.

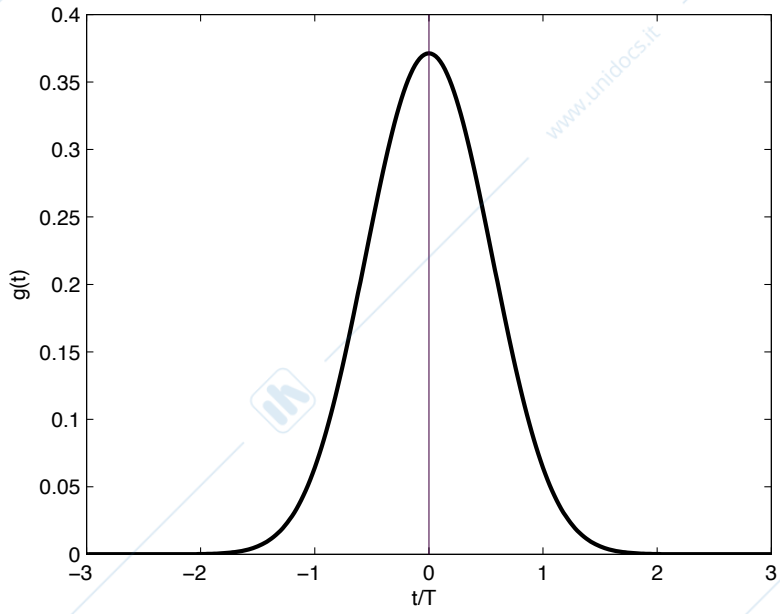

Figure 4.16: GMSK pulse.

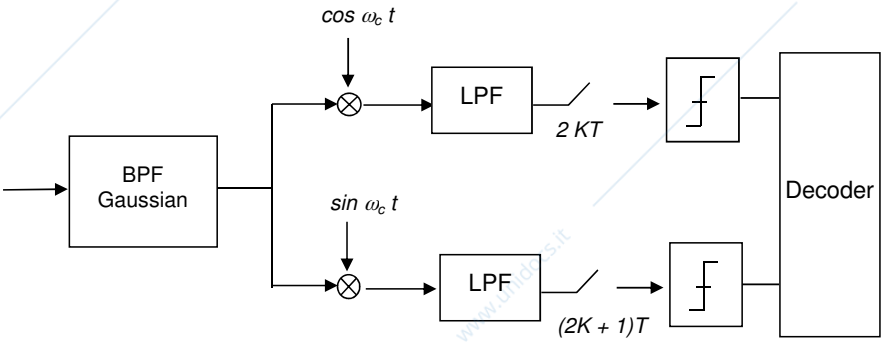

Figure 4.17: GMSK sub-optimal demodulator.

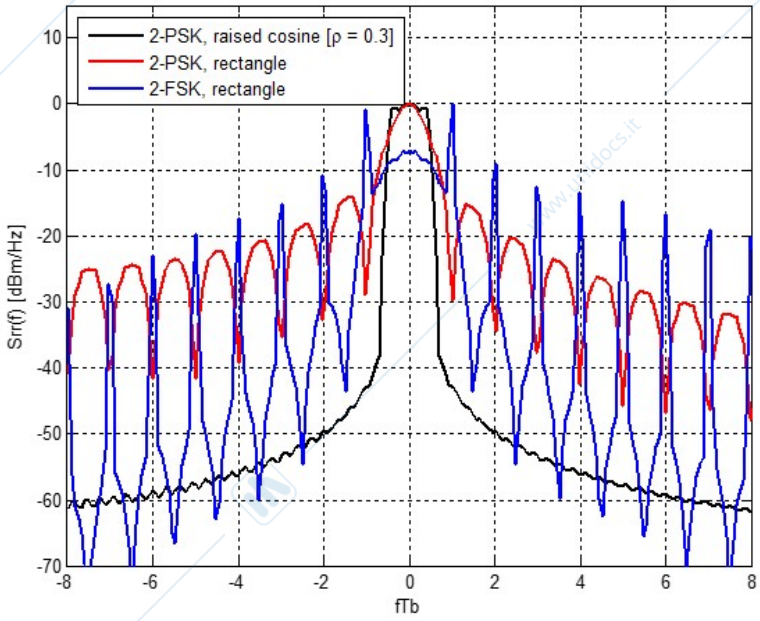

Figure 4.18: Power spectral density of BPSK and FSK.

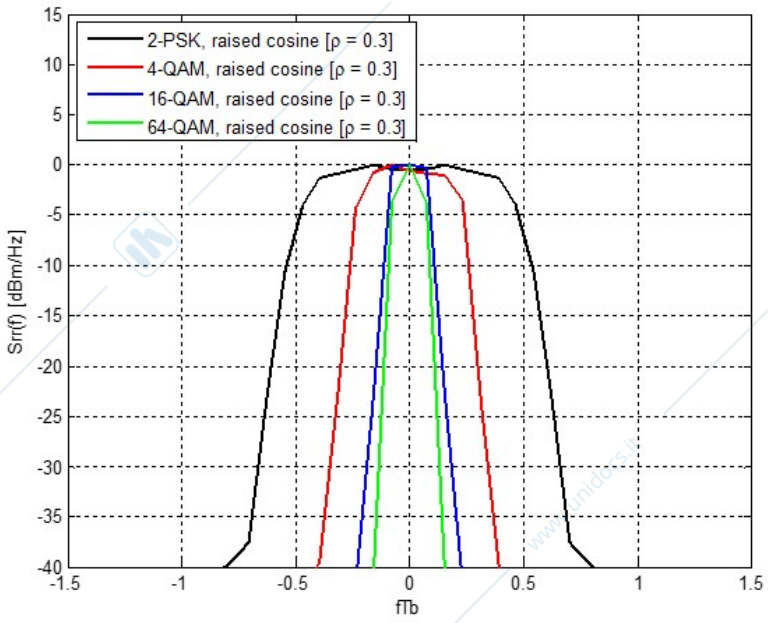

Figure 4.19: Power spectral density of BPSK and M-QAM with a root raised cosine pulse.

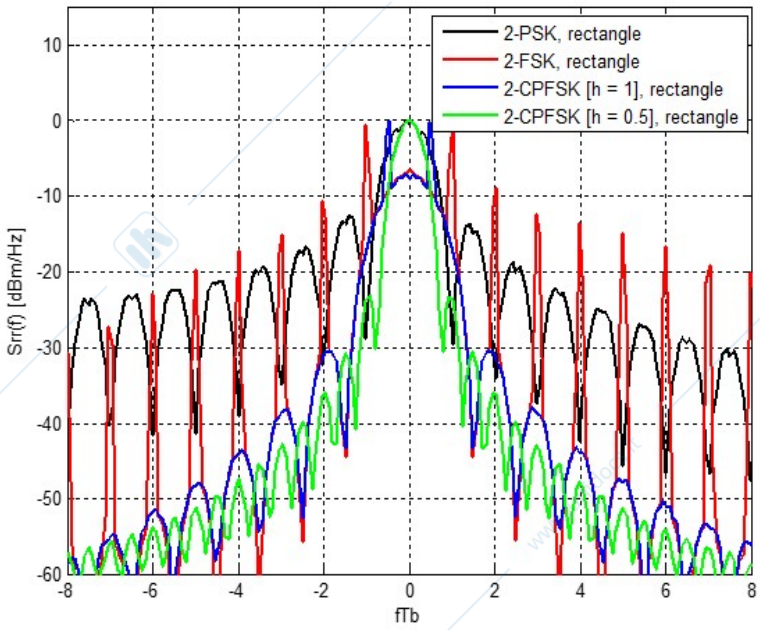

Figure 4.20: Power spectral density of BPSK, FSK and CPFSK.

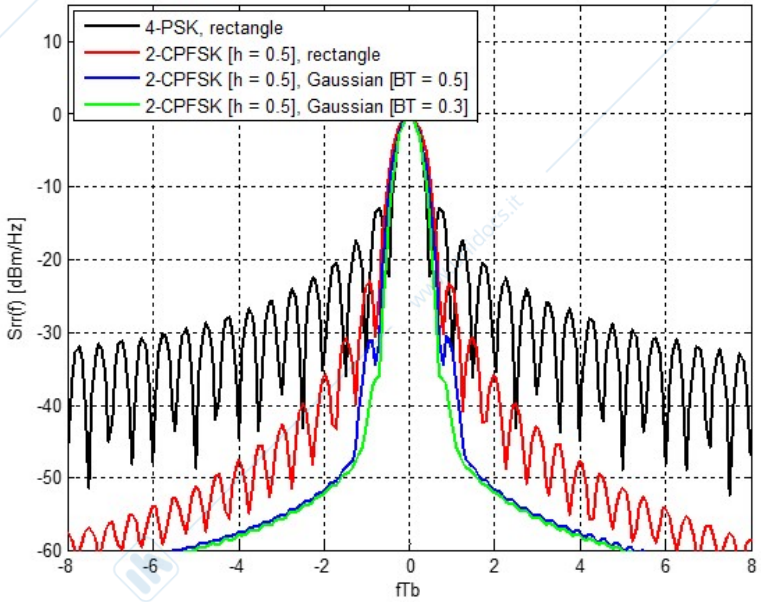

Figure 4.21: Power spectral density of QPSK, CPFSK with and without Gaussian filtering.

Modulation method	Spectral efficiency for 90% bandwidth	Spectral efficiency for 99% bandwidth
BPSK	0.59	0.05
QPSK, OQPSK	1.18	0.10
MSK	1.29	0.85
GMSK (BT = 0.5)	1.45	0.97
QAM (roll-off = 0.5)	2.04	1.58

Figure 4.22: Spectral efficiency of different modulations and pulses.